Electronic Supporting Information (ESI)

Single-Ion Magnetism in Novel Btp-Based Cobalt complexes of Different Charge

Gustavo Rama-Martínez,[a,‡] Marcelo Osorio-Celis,[a,‡] Yolanda Sabater-Algarra,[a] Diego Sánchez-Brunete,[a] Antonio L. Llamas-Saiz,[c] Eugenia P. Quirós-Díez,[a] M. Eugenio Vázquez,[b] Miguel Vázquez López[a] and María del Carmen Giménez López[a,*]

[a.] *Centro Singular de Investigación en Química Biolóxica e Materiais Moleculares (CiQUS) and Departamento de Química Inorgánica, Universidade de Santiago de Compostela. 15782 Santiago de Compostela, Spain.*
[b.] *Centro Singular de Investigación en Química Biolóxica e Materiais Moleculares (CiQUS) and Departamento de Química Orgánica, Universidade de Santiago de Compostela. 15782 Santiago de Compostela, Spain.*
[c.] *Unidade de Raios X. Área de Infraestruturas de Investigación, Universidade de Santiago de Compostela, 15782 Santiago de Compostela, Spain.*
* maría.gimenez.lopez@usc.es

Authors contributions

The following table details the contribution of each author according to the Contributor Roles Taxonomy (CRediT). The degree of contribution is coded as lead (black), equal (dark grey), or supporting (light grey).

	GRM	MOC	YSA	DSB	ALLS	EPQD	AGB	MEV	MVL	MCGL
Conceptualization: Ideas formulation or evolution of overarching research goals.										
Methodology: Development or design of methodology; creation of models.										
Validation: Verification of the overall reproducibility of results and research outputs										
Formal Analysis: Application of formal techniques to analyze the data.										
Investigation: Synthesis of the ligands and metal complexes.										
Investigation: Metal binding studies										
Investigation: Structural analysis										
Investigation: Magnetic data analysis										
Resources: Provision of reagents, materials, instrumentation, and analysis tools.										
Data Curation: Management to annotate, scrub and maintain research data.										
Writing: Original Draft: Preparation of the paper, specifically writing the initial draft.										
Writing: Review & Editing: Critical review, commentary, or revision.										
Visualization: Preparation, of the paper, specifically visualization &/or presentation										
Supervision: Oversight responsibility for the research planning & execution.										
Project Administration: Management and coordination of the research.										
Funding Acquisition: Acquisition of the financial support leading to this publication.										

Experimental procedures

NMR spectra were recorded on *Bruker AMX500 11.74 T* (500 MHz) spectrometer and referenced to the residual signal of the solvent. **RP-UHPLC-MS** analysis were carried out in an *Agilent Technologies 1260 Infinity III* chromatograph in tandem with an *Agilent Technologies 6120* mass spectrometer, using gradient elution (5-95% B) of the mobile phase (A: H_2O 0.1% TFA; B: ACN 0.1% TFA). **MS-ESI-TOF** data were recorded on a *Bruker Microtof ESI-TOF* instrument at 298 K with a scan range of m/z 100-2000 in positive mode. **Infra-red spectra** were measured using a *Bruker Alpha FTIR* spectrometer with a platinum ATR module. **TGA measurements** were performed on a *Mettler Toledo TGA/DSC 3+ STAR^e* system analyzer coupled to a robot. **Single-crystal X-ray diffraction** measurements were performed on a *Bruker D8 Venture Photon 100 CMOS κ-geometry* diffractometer system equipped with an Incoatec high brilliance IμS microsource (MoKα, λ = 0.71073 Å) and an *Incoatec HeliosTM* multilayer optics monochromator. The labels for compounds **1** and **3** correspond to the numbering of atoms, starting from atom 1 to the last atom. However, for compound **2**, which has two metallic centers, the labeling is based on the number of ligands per metallic center. N1_1 and N1_2 represent the two pyridine nitrogen atoms, one for each ligand bound to Co1. The **X-ray powder diffraction (XRPD)** data were collected in Bragg-Brentano geometry using a Bruker D8 Advance X-ray diffractometer (40 kV, 40 mA, theta/theta) equipped with a sealed Cu X-ray tube (CuKα1 (λ = 1.5406 Å)). The **magnetic susceptibility measurements** were performed using a *Quantum Design MPMS-XL-7 SQUID* magnetometer equipped with a 7 T magnet. Magnetic parameters from static measurements (D and E) were fitted using PHI software package using as input the experimental data. Note: A combined orbital reduction parameter is also included. Typical values of α for a six-coordinate high-spin Co(II) ion fall within the range of 0.70-1. The spin-orbit coupling constant, λ_{SO}, is expected to range from 90 to 180 cm^{-1} for six-coordinate octahedral Co(II) complexes.[1] To avoid overparameterization when fitting experimental data, α was fixed at -1 and λ_{SO} was initially fixed at 170 cm^{-1}, values close to that of the free Co(II) ion. However, the values for D and E gave nonsensical results, so α and λ_{SO} were consider as a free parameter, and it was confirmed that the values, after adjusting D and E, remained within the expected experimental range. α for **1** is -1.05 and for **3** -1.34, and λ_{SO} for **1** is -188.7 and for **3**, -170. The orbital reduction parameter is slightly larger for **3** than for **1**, indicating a stronger ligand field in the case of **3**.

Synthesis of 2,6-bis((trimethylsilyl)ethynyl)pyridine (7)

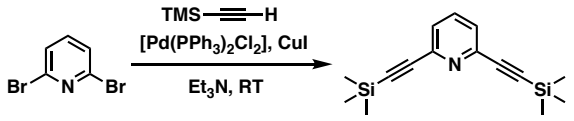

A 250 mL round bottom flask, connected to the Schenk line under N_2 atmosphere, was charged with 2.28 g of 2,6-dibromopyridine (9.65 mmol, 1 eq.), CuI (37.0 mg, 0.2 mmol, 0.02 eq.), $[PdCl_2(PPh_3)_2]$ (135.0 mg, 0.2 mmol, 0.02 eq.) and 40 mL of TEA. While passing a current of N_2, trimethyllsilylacetylene (2.80 mL, 20.3 mmol, 2.1 eq.) was added to the mixture and the reaction was stirred at room temperature overnight. A saturated solution of NH_4Cl was added and the mixture was stirred for 30 min. The aqueous layer was extracted with Et_2O (3 × 30 mL). The combined organic extracts were washed with brine (80 mL), dried with $MgSO_4$ and the solvent removed under vacuum. The residue was purified by flash chromatography (silica gel, hexane:ether 7:3) to afford **7** as a white solid (2.515 g, 96% yield). **^{1}H-NMR** (500 MHz, $CDCl_3$, δ): 7.55 (t, ^3J = 7.8 Hz, 1H), 7.34 (d, ^3J = 7.8 Hz, 2H), 0.22 (s, 18H); **^{13}C-NMR** (126 MHz, $CDCl_3$, δ): 143.40, 136.32, 126.73, 103.19, 95.46, 0.26; **DEPT-135** (126 MHz, $CDCl_3$, δ): 136.32, 126.73, 0.26; **MS-ESI:** Calculated for $[C_{15}H_{22}NSi_2]^+$ 272.13, found 272.17

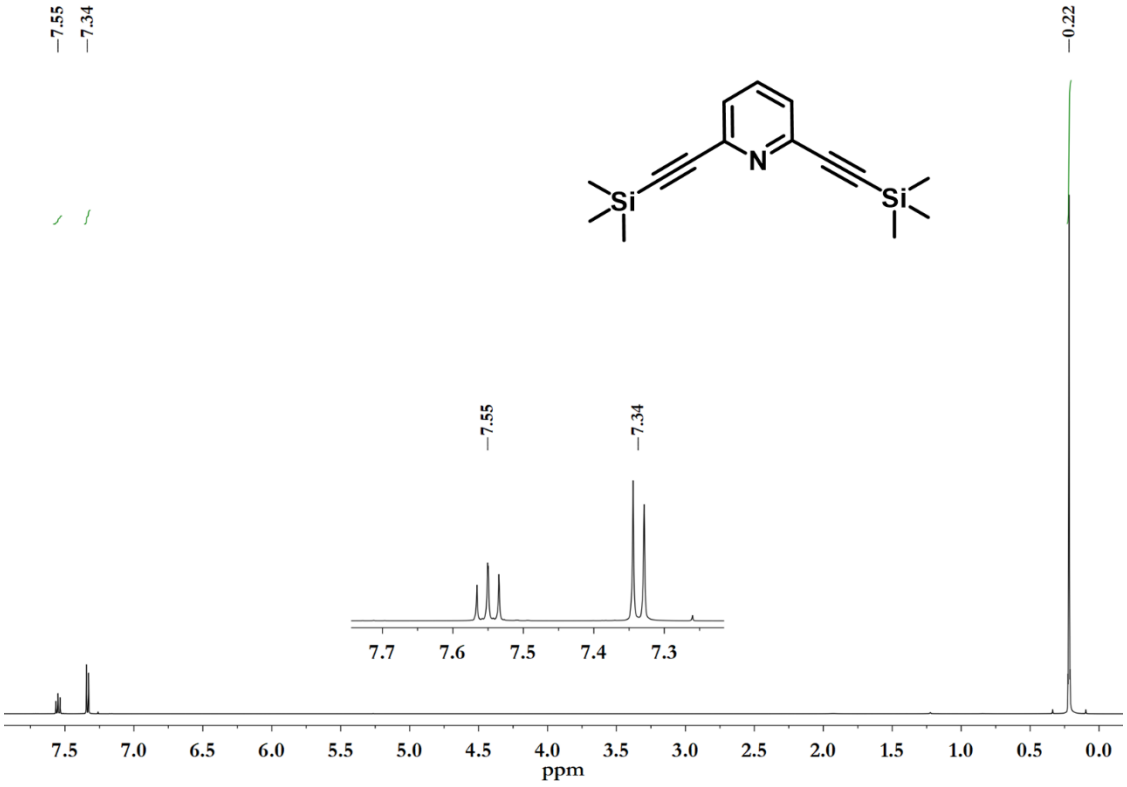

*Figure S1. ^{1}H NMR spectrum of **7** in $CDCl_3$.*

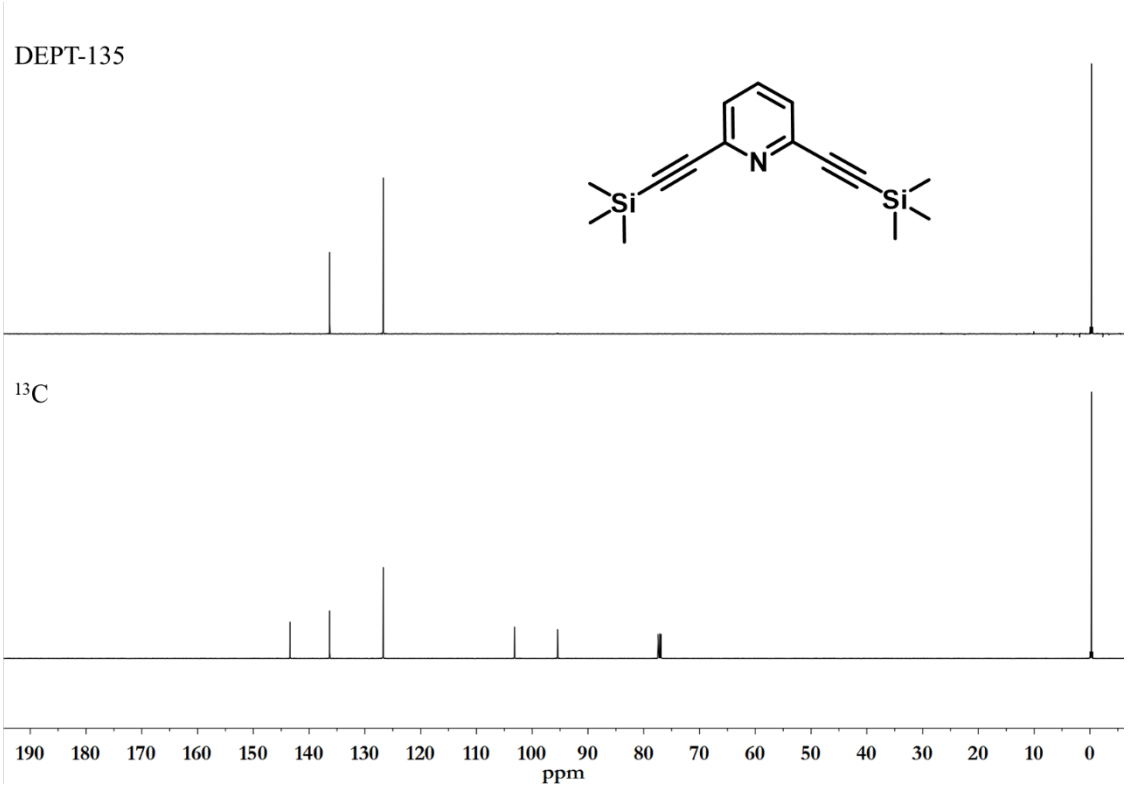

*Figure S2. ^{13}C-DEPT 135 spectra of **7** in $CDCl_3$.*

Synthesis of tert-butyl 2-azidoacetate (8)

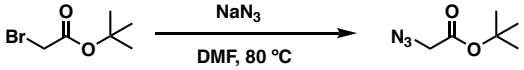

A 250 mL round bottom flask was charged with a solution of 5.00 mL of *tert*-butyl bromoacetate (6.65 g, 34.1 mmol, 1 eq.) in 50 mL of DMF, 11.1 g of NaN_3 (170.5 mmol, 5 eq.) were added at RT. The mixture was stirred under inert atmosphere for 30 h when, 100 mL of water were added and the mixture was extracted with diethyl ether (3 × 40 mL), the combined organic phase was washed with water (2 × 40 mL), 1 M LiCl (2 × 40 mL) and dried over anhydrous $MgSO_4$. The solvent was removed, and the colorless oil was dried under vacuum to give **8** with no further purification (5.04 g, 94% yield). **^{1}H-NMR** (500 MHz, $CDCl_3$, δ): 3.69 (s, 2H), 1.44 (s, 9H); **^{13}C-NMR** (126 MHz, $CDCl_3$, δ): 167.73, 82.92, 50.86, 27.96; **DEPT-135** (126 MHz, $CDCl_3$, δ): 50.86 (CH_2), 27.96 (CH_3); **IR** ν_{max}/cm^{-1} = 2103 (N_3), 1738 (C=O)

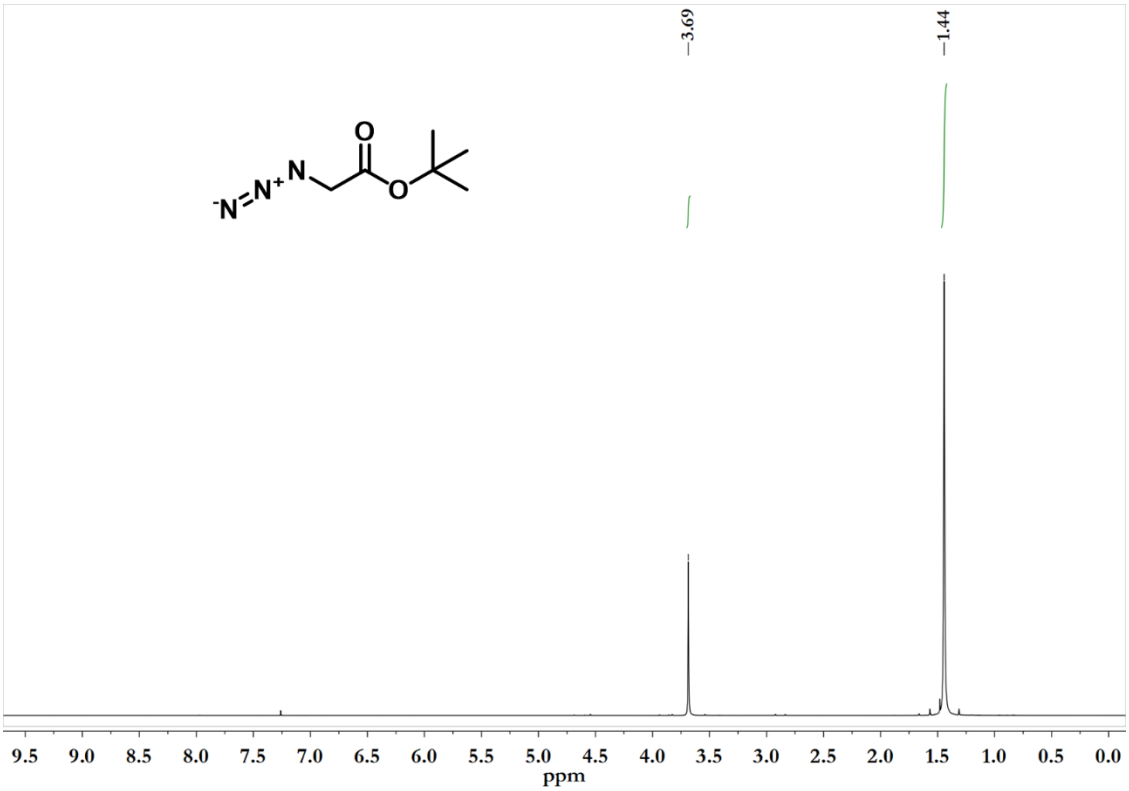

*Figure S3. ^{1}H-NMR spectrum of **8** in $CDCl_3$.*

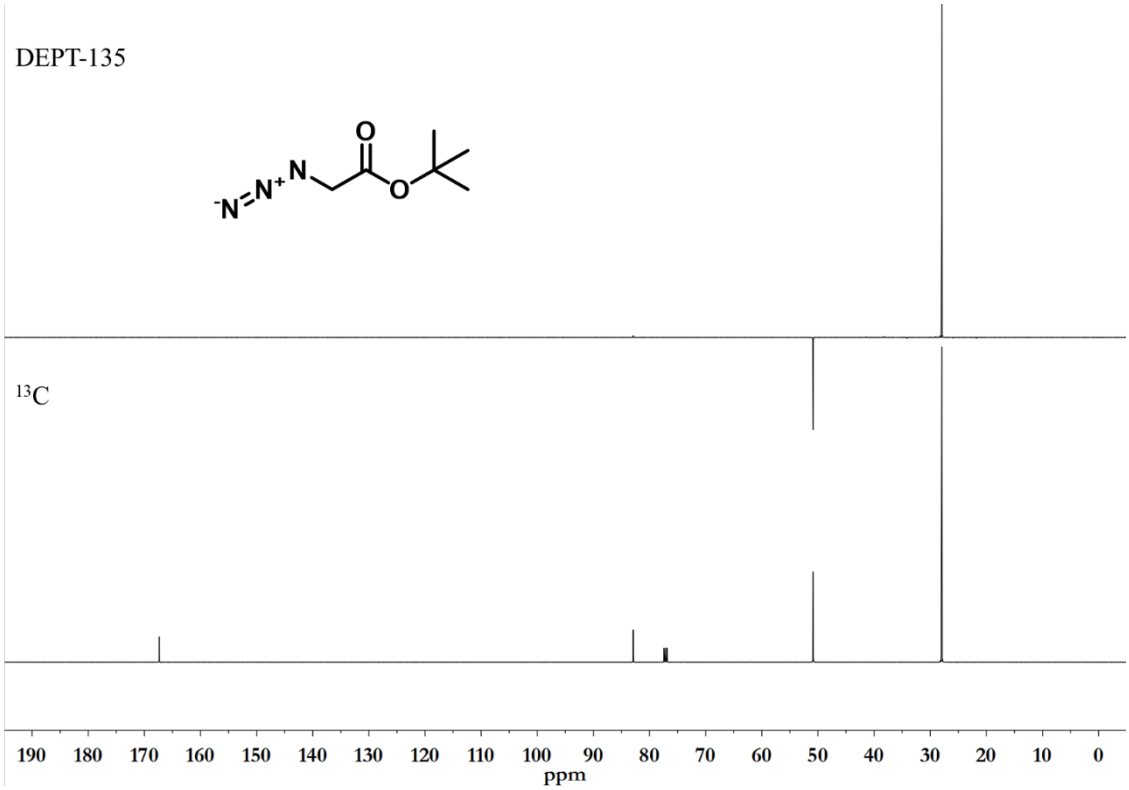

*Figure S4. ^{13}C-DEPT 135 spectra of **8** in $CDCl_3$.*

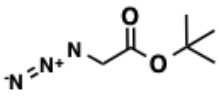

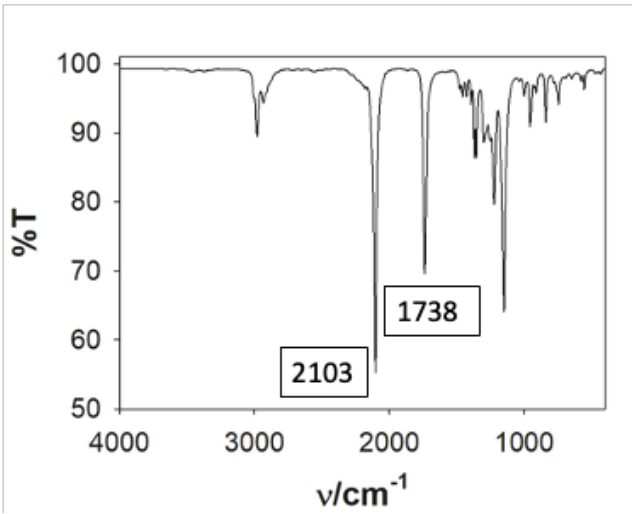

*Figure S5: FTIR of **8**, highlighting the bands at 2103 cm^{-1} (N_3) and 1738 cm^{-1} (C=O).*

Synthesis of ^{tBuOOC}Btp

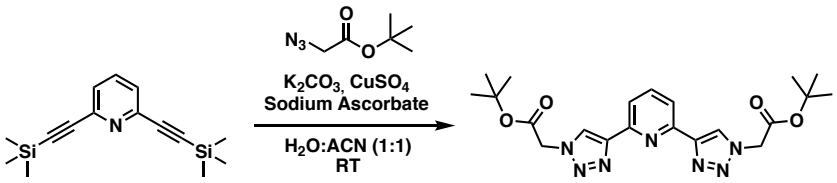

A 100 mL round bottom flask charged with 624.6 mg of **7** (2.3 mmol, 1 eq.), K_2CO_3 (1.272 g, 9.2 mmol, 4.0 eq.), sodium ascorbate (182.3 mg, 0.98 mmol, 0.4 eq.), $CuSO_4 \cdot 5H_2O$ (69.9 mg, 0.28 mmol, 0.2 eq.), 903.7 mg of **8** (5.75 mmol, 2.5 eq.) and 0.720 mL of N,N'-diisopropylethylamine DIPEA (4.2 mmol, 3 eq.) were suspended in a mixture of CH_3CN:H_2O (1:1) under inert atmosphere. The mixture was stirred under N_2 atmosphere for 16 hours at room temperature, then a saturated solution of NH_4Cl was added and the mixture was stirred for 30 min, the white solid was isolated by filtration, washed with isopropyl alcohol, and deionized water and freeze-dried to give ^{tBuOOC}**Btp** as a white solid (893.6 mg, 88% yield). **^{1}H-NMR** (500 MHz, $CDCl_3$, δ): 8.67 (s, 2H), 8.00 (s, 3H), 5.39 (s, 4H), 1.46 (s, 18H); **^{13}C-NMR** (126 MHz, DMSO-d_6, δ): 116.19, 149.81, 147.06, 138.38, 124.96, 118.51, 82.52, 51.14, 27.64; **DEPT-135** (126 MHz, DMSO-d_6, δ): 138.38 (CH), 124.96 (CH), 118.51 (CH), 51.14(CH_2), 27.64 (CH_3)**; MS-ESI:** m/z calculated for $[C_{13}H_{12}N_7O_4]^+$ 442.22, found 442.24

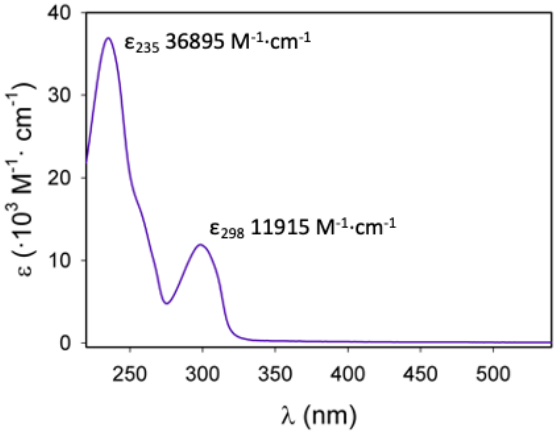

*Figure S6: UV-visible spectrum of ^{tBuOOC}**Btp** in CH_3OH at 293 K.*

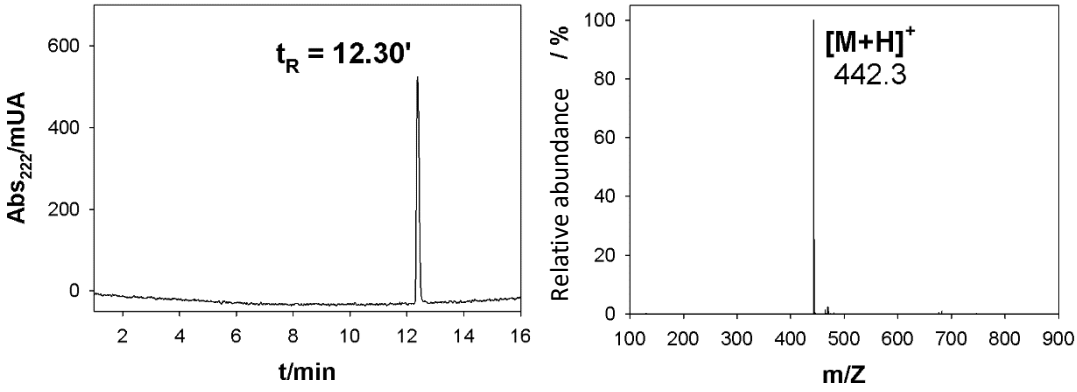

*Figure S7: Left, RP-UHPLC of ^{tBuOOC}**Btp** (5-95%B 15 min; A = H_2O 0.1% TFA, B = CH_3CN, 0.1% TFA); right, ESI-MS corresponding to the chromatographic peak at 12.30 min.*

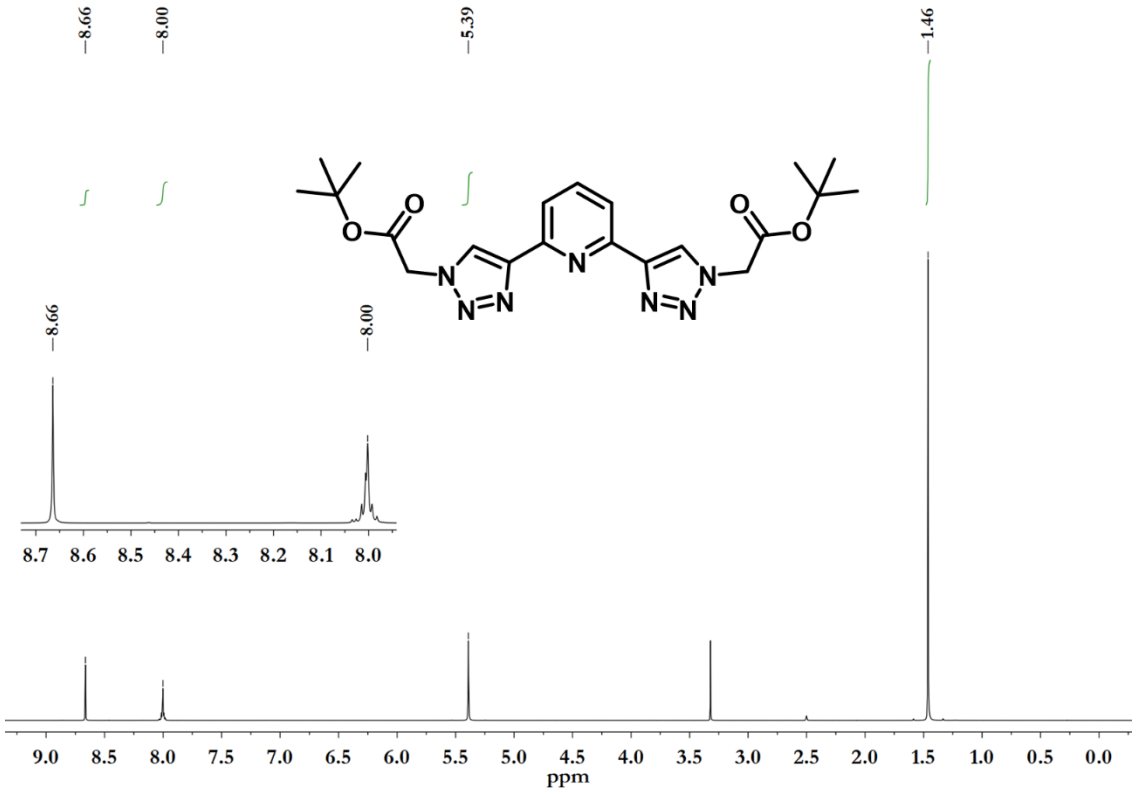

Figure S8. ^{1}H-NMR spectrum of ^{tBuOOC}***Btp*** *in DMSO-d_6.*

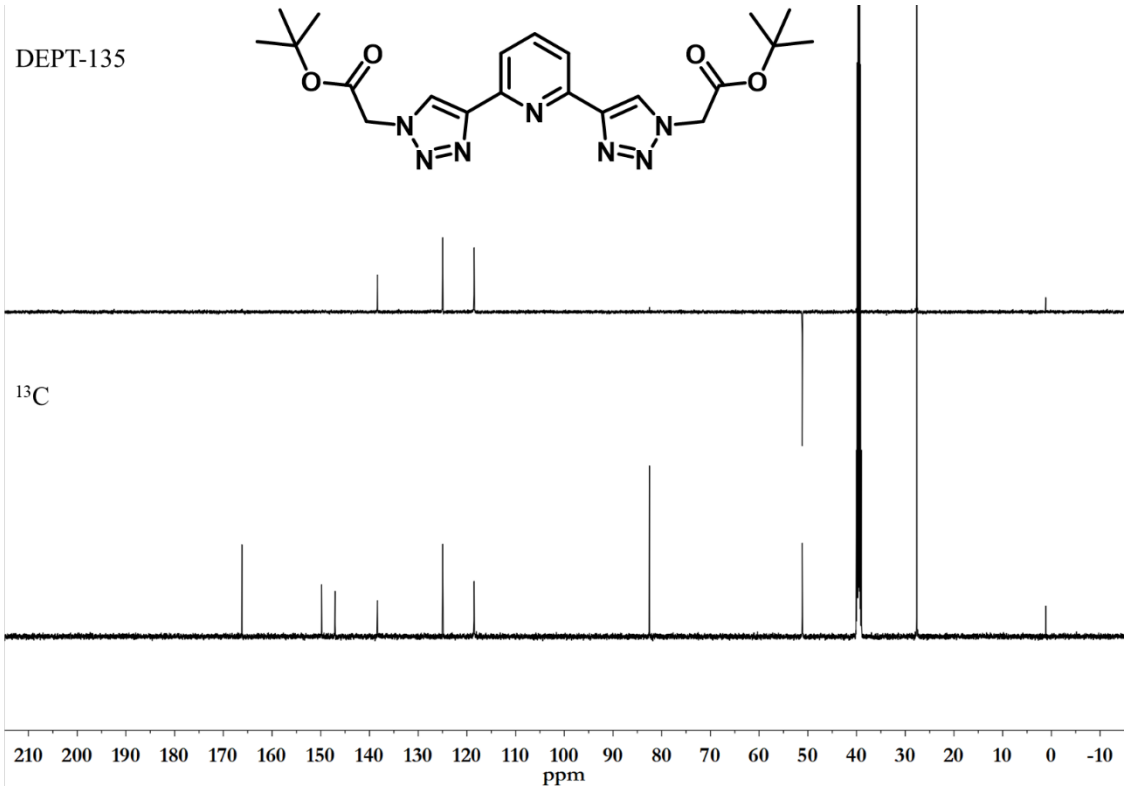

Figure S9. ^{13}C-DEPT 135 spectra of ^{tBOOC}***Btp*** *in DMSO-d_6.*

Synthesis of ^{HOOC}Btp

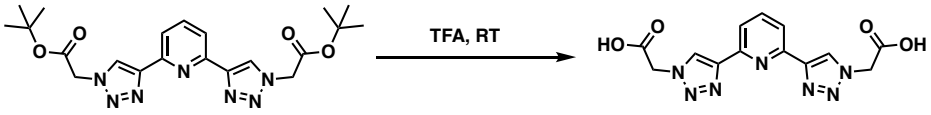

In a 100 mL round bottom flask, which contains 513.0 mg of ^{tBuOOC}**Btp** (1.16 mmol), 5 mL of cold trifluoroacetic acid were added. The solution was stirred at RT for 60 minutes then, 60 mL of Et_2O were added dropwise under vigorous stirring and a powdered white solid appeared. The solid was isolated by filtration, washed with Et_2O (3 × 15 mL) and dried under vacuum. (376.9 mg, 98.5% yield). **^{1}H-NMR** (500 MHz, DMSO-d_6, δ): 13.49 (br, 1H), 8.66 (s, 2H), 7.99 (m, 3H), 5.39 (s, 4H); **^{13}C-NMR** (126 MHz, DMSO-d_6, δ): 168.54, 149.85, 147.06, 138.39, 124.96, 118.48, 50.74; **DEPT-135** (126 MHz, DMSO-d_6, δ): 138.39 (CH), 124.96 (CH), 118.48 (CH), 50,74 (CH_2); **MS-ESI:** m/z calculated for $[C_{13}H_{12}N_7O_4]^+$ 330.09, found 330.11.

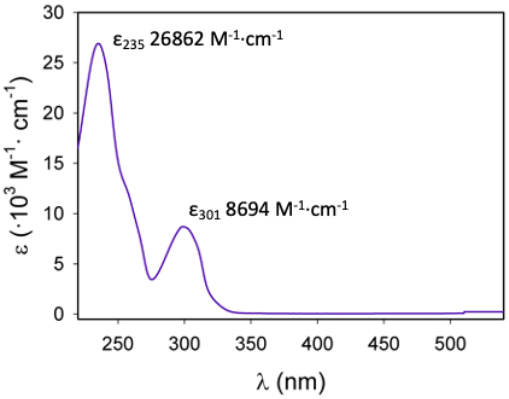

*Figure S10: UV-visible spectrum of the ligand ^{HOOC}**Btp** in CH_3OH at 293 K.*

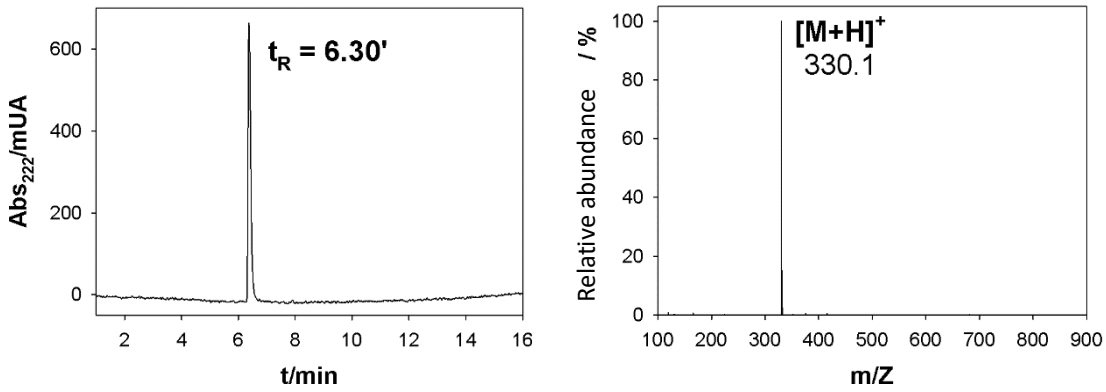

*Figure S11: Left, RP-UHPLC of the ligand ^{HOOC}**Btp** (5-95% B 15 min; A = H_2O 0.1% TFA, B =CH_3CN, 0.1% TFA); right, ESI-MS corresponding to the chromatographic peak at 6.30 min.*

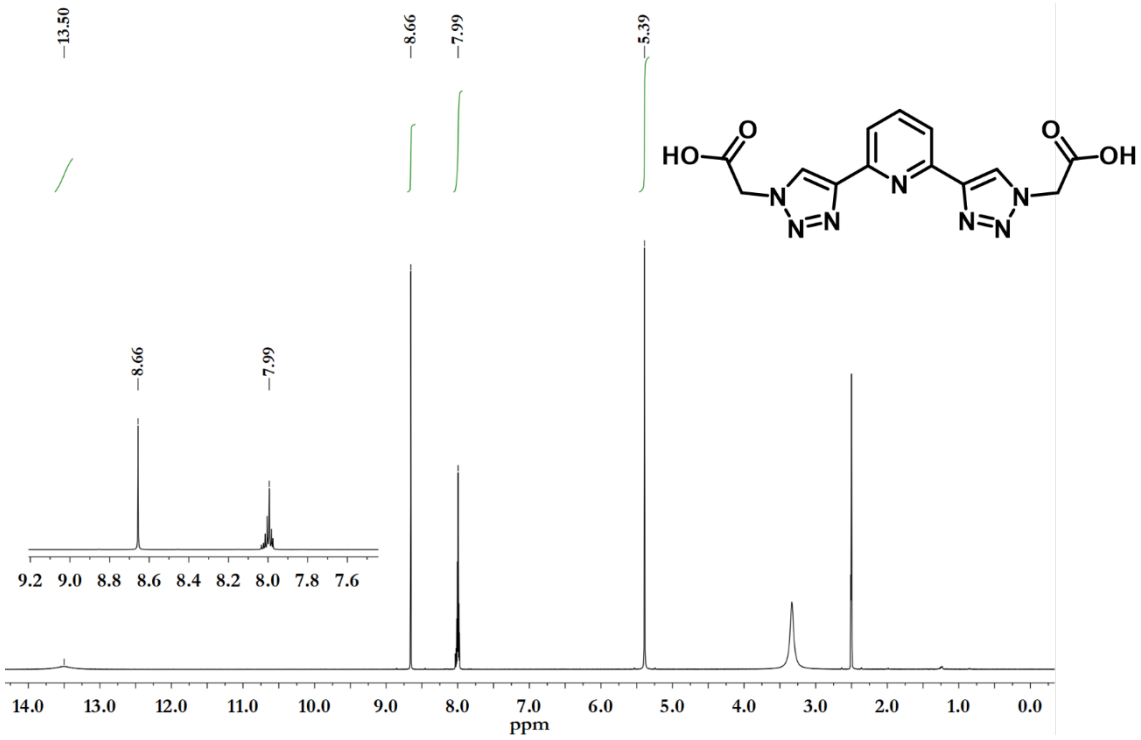

Figure S12. ^{1}H-NMR spectrum of ligand ***^{HOOC}Btp*** *in DMSO-d_6.*

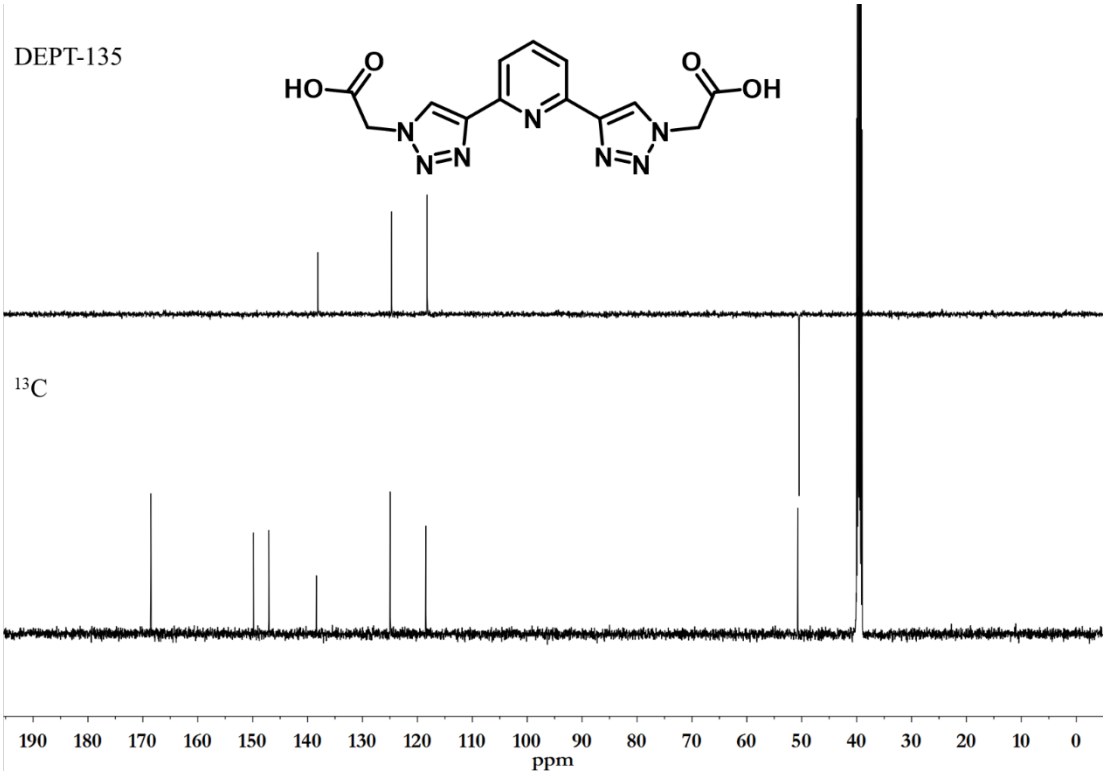

Figure S13. ^{13}C-DEPT 135 spectra of ligand ***^{HOOC}Btp*** *in DMSO-d_6.*

UV-Vis studies

Extinction coefficient (ε) of the ligands

^{HOOC}Btp: λ_{max} (methanol)/nm (ε/M^{-1} cm^{-1}) 235 (**26862**) and 301 (**8694**)
λ_{max} (water)/nm (ε/M^{-1} cm^{-1}) 232 (**19640**) and 299 (**7459**)
^{tBuOOC}Btp: λ_{max} (methanol)/nm (ε/M^{-1} cm^{-1}) 234 (**36895**) and 299 (**11915**)

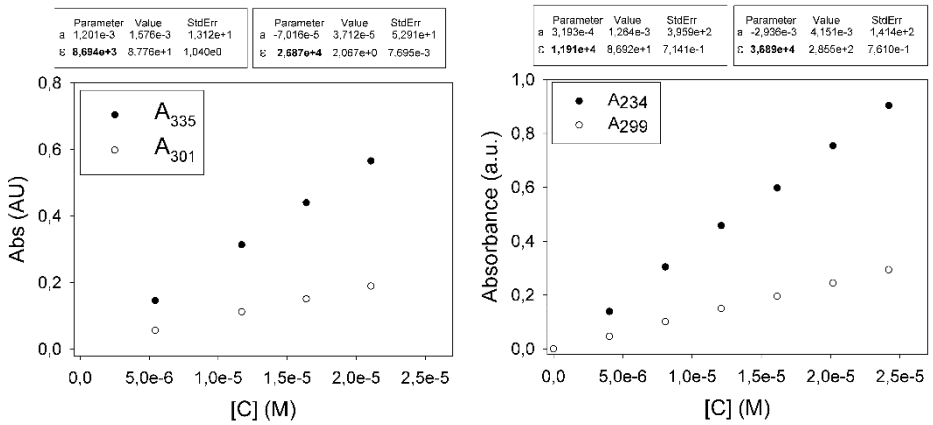

Figure S14: Left, concentration vs. absorbance plot to calculate the extinction coefficient of ***^{HOOC}Btp*** *in CH_3OH; right, concentration vs. absorbance plot to calculate the extinction coefficient of* ***^{tBuOOC}Btp*** *in CH_3OH.*

Titrations experiments in CH_3OH

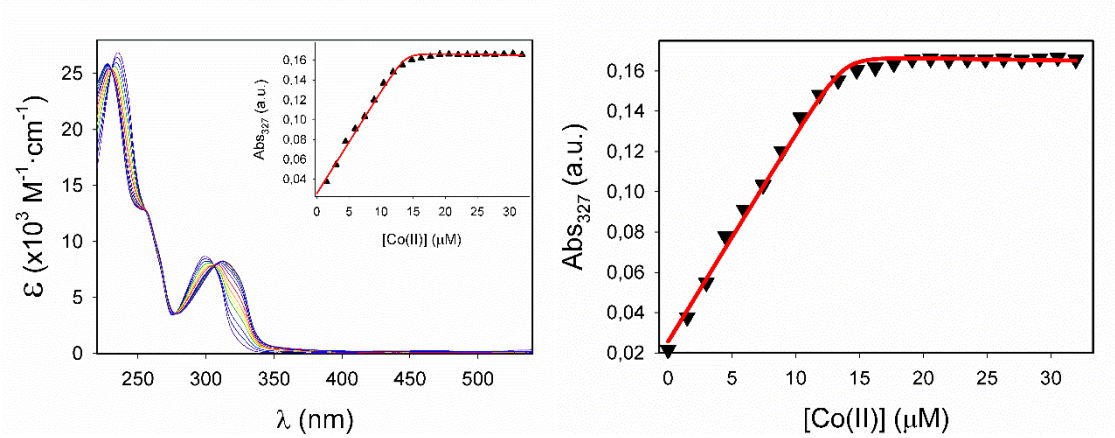

Figure S15: UV-vis titration of ***^{HOOC}Btp*** *(25 µM) versus Co^{II} 4.5 µL addition (1 mM); inset, titration profile Abs_{327} vs $[Co^{II}]$.*

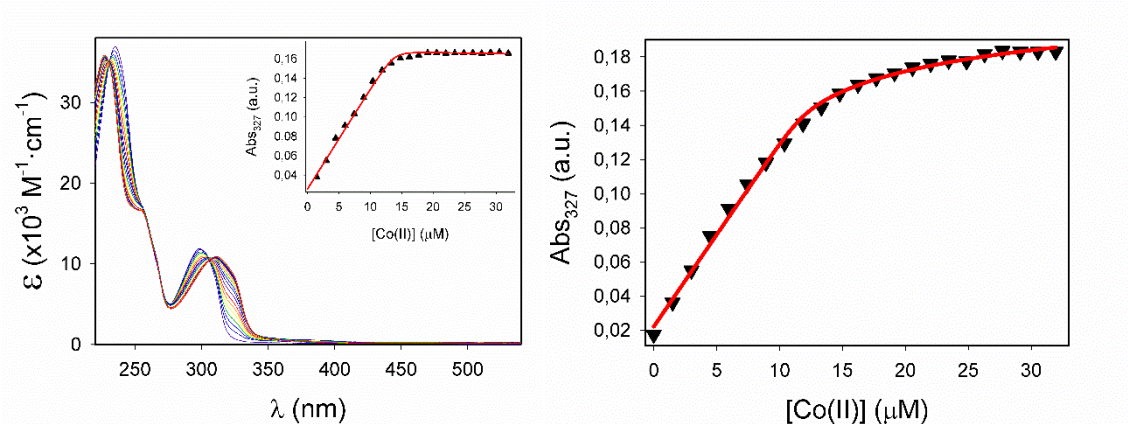

Figure S16: UV-vis titration of ^{tBuOOC}***Btp*** *(25 µM) versus Co^{II} 4.5 µL addition (1 mM); inset, titration profile Abs$_{327}$ vs [Co^{II}].*

Fluorescence studies

Titrations experiments in CH_3OH

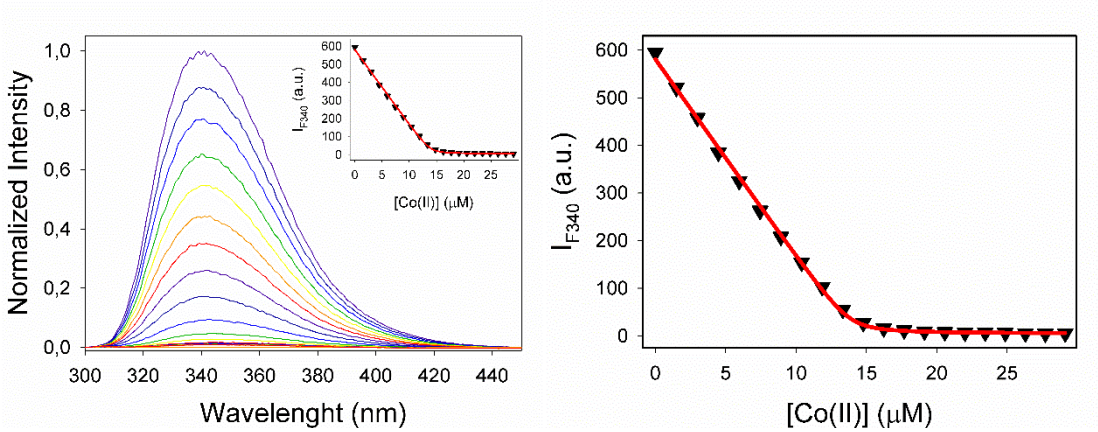

Figure S17: Fluorescence quenching titration of ^{HOOC}***Btp*** *(25 µM) versus Co^{II} 4.5 µL addition (1 mM); inset, titration profile emission intensity at 340 nm vs [Co^{II}].*

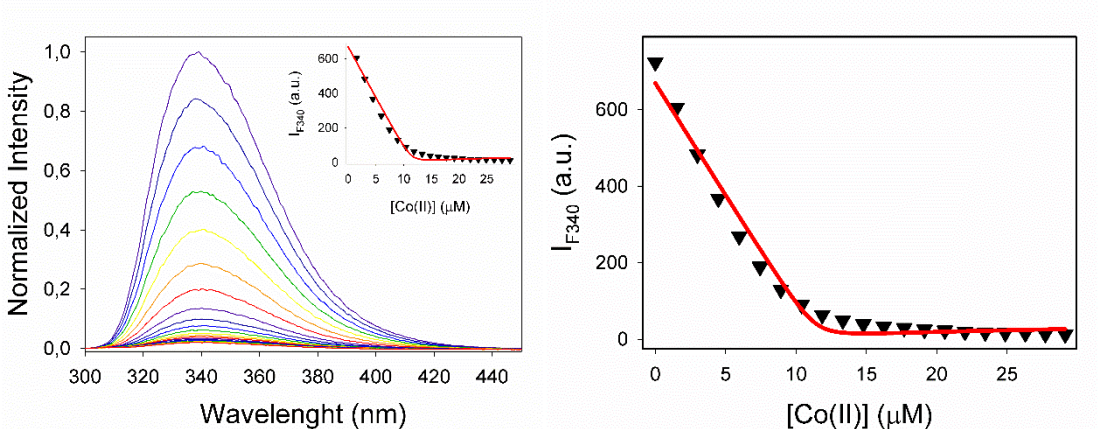

Figure S18: Fluorescence quenching titration of ^{tBuOOC}***Btp*** *(25 µM) versus Co^{II} 4.5 µL addition (1 mM); inset, titration profile emission intensity at 340 nm vs [Co^{II}].*

DynaFit analysis

Experimental data were fitted with the DynaFit 4.0 software, which performs a numerical treatment of the system. The program is available free of charge for academia at http://www.biokin.com/dynafit/

Dynafit requires plain text files called scripts that contain information about the chemical model underlying the experimental data, the values of model parameters, such as starting concentrations of reactants, as well as information about location of the files. A typical script used in the analysis titrations is included below. The file has been commented to indicate the purpose of the keywords and sections, but the reader is recommended to review the DynaFit scripting manual distributed along the program or available at the DynaFit website.

```
[task]                          ;semicolons indicate comments from actual instructions
  task   =  fit                 ;nature of the calculation to be performed
  data  =  equilibria
[mechanism]                     ;Free-form 1:2 (M:L) binding model with K1 and K2
  M   +  L  <==>   ML :   K1    ;to be calculated as association constant
  assoc
  ML +  L  <==>  ML2 : K2
  assoc
[constants]                     ;Initial values for step formation constants (Kn) for iteration
  K1 =  8 ?                     ;the "?" indicates that this will be optimized
  K2 =  5 ?
[concentrations]
  L = 25.0                      ;Fixed conc. of the ligand during the metal titration (µM)
[responses]                     ;contribution to the spectroscopic signal of each
  M     =   0 ?                 ;of the different components of the equilibrium
  ML   =   6 ?                  ;these will be optimized ("?" after the values).
  ML2 =  10 ?
[data]                          ;location of files and information about the data
  variable   M                  ;the species that changes conc. during the titration
  offset auto ?
  directory                     ;file path (relative to DynaFit program location)
  ./exp/ConstantsBtp
  extension txt
  file f1                       ;name of the experimental data file
[output]
  directory ./exp/hel/out       ;path indicating location of DynaFit output file
```

Thermogravimetric analysis

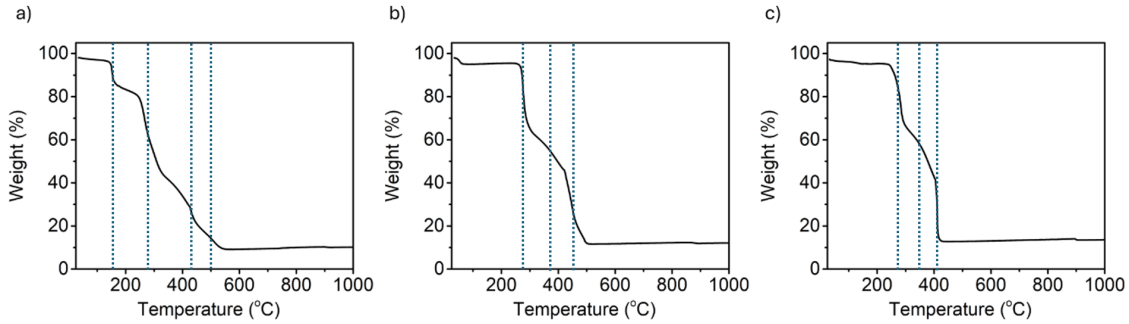

Figure S19. Thermogravimetric analysis (TGA) on the collected single crystals of **1** (a), **2** (b) and **3** (c) under dry air in the range of 40-1000 °C with a scan rate of 2 °C/min.

Single Crystal X-Ray Diffraction

*Table S1: Single-crystal X-ray diffraction data of **1**–**3** at 100 K.*

	1	**2**	**3**
Chemical Formula	$C_{44}H_{62}Cl_2CoN_{14}O_{18}$	$C_{26}H_{27}ClCoN_{14}O_{15}$	$C_{28}H_{29}CoN_{15}O_{11}$
Size (mm)	0.171x 0.155 x 0.099	0.020 x 0.050 x 0.060	0.181 x 0.188 x 0.278
Formula weight (g/mol)	1204.90	869.99	810.59
Crystal system	Triclinic	Triclinic	Triclinic
Space group	$P\bar{1}$	$P\bar{1}$	$P\bar{1}$
a [Å]	12.4084(3)	10.8758(10)	10.8428(5)
b [Å]	15.0996(4)	15.7999(14)	12.8667(6)
c [Å]	17.2362(5)	22.4832(18)	13.2049(7)
α [°]	70.5260(10)	102.685(3)	71.4184(17)
β [°]	76.1110(10)	100.768(3)	72.7316(16)
γ [°]	70.2810(10)	106.576(3)	81.3449(17)
V [Å^3]	2836.36(13)	3481.5(5)	1664.30(14)
Z	2	4	2
Dx [mg/m^3]	1.411	1.660	1.618
Temperature [K]	100	100	100
Tmax/Tmin	0.9550, 0.9240	0.990, 0.900	0.8990, 0.8510
Absortion coeff. [mm^{-1}]	0.477	0.662	0.601
F (000)	1186	1780	834
Θ range [°]	2.21 to 30.07	2.8108 to 21.2166	2.00 to 37.84
Reflections collected	99182	139579	32366
Independent reflections	16592	12733	28539
GOF on F^2	1.022	1.054	1.142
Final R indices [I > 2σ(I)]	R1 = 0.0415, wR2 = 0.0834	R1 = 0.0737, wR2 = 0.1913	R1 = 0.0488, wR2 = 0.1138
***R* indices (all data)**	R1 = 0.0629 wR2 = 0.0929	R1 = 0.1161 wR2 = 0.2200	R1 = 0.0681 wR2 = 0.1280

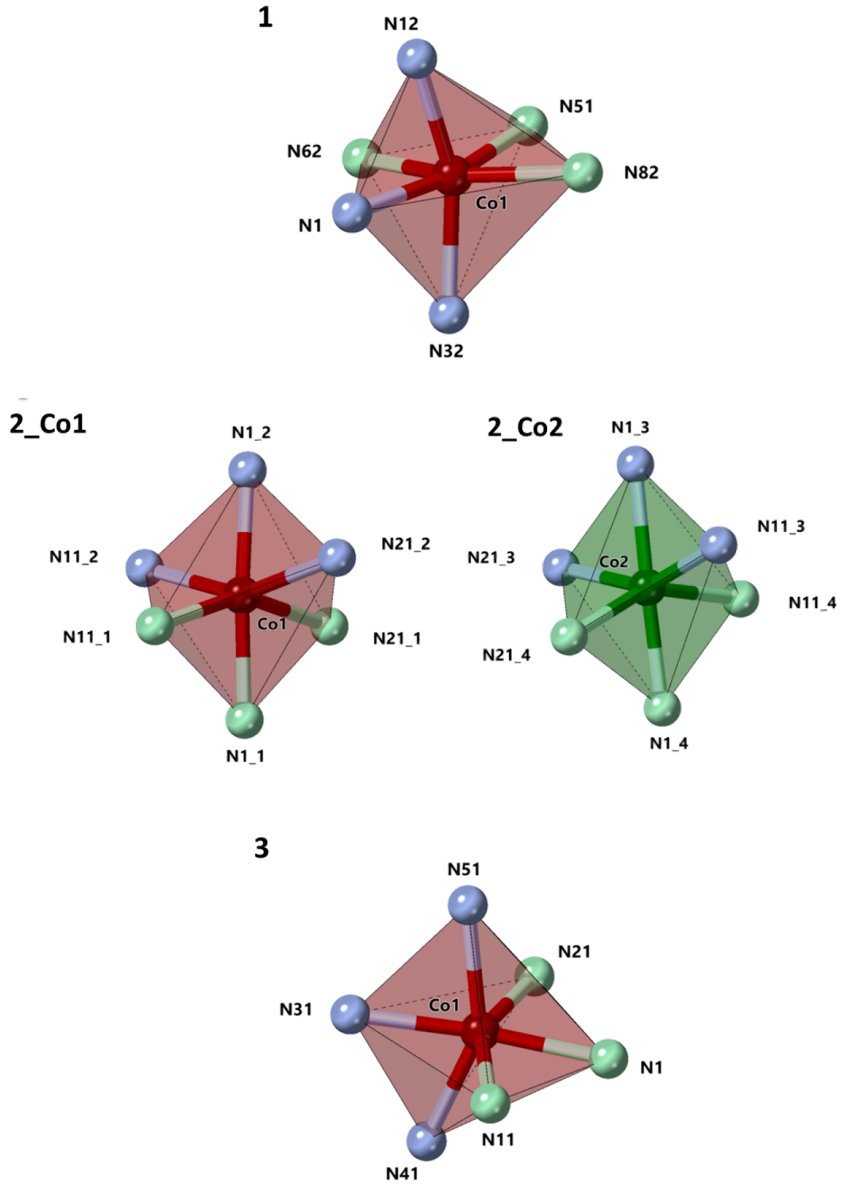

*Scheme S1. Crystallographic representations showing the deviation of the [$Co^{II}N_6$] environment from a regular octahedral coordination geometry for complexes **1**–**3**, where the disposition of the N atoms around the Co^{II} center is shown. Light blue and light green nitrogen atoms are referred to each ligand.*

*Table S2: Co–N bond distances for **1**–**3** at 100 K. Because of the $N_{Triazole}$ disorder distances of Co2-N21_4b and Co2-N21_4c has been omitted. Representations was performed taking into account the atoms with the higher occupational factor.*

1		2_Co1		2_Co2		3	
Co-N	**Lenght (Å)**	**Co-N**	**Lenght (Å)**	**Co-N**	**Lenght (Å)**	**Co-N**	**Lenght (Å)**
Co1-N1	2.1025(14)	Co1-N1_2	2.098(4)	Co2-N1_3	2.099(5)	Co1-N1	2.0913(14)
Co1-N32	2.1380(14)	Co1-N21_2	2.139(5)	Co2-N21_3	2.139(5)	Co1-N21	2.1588(17)
Co1-N12	2.1202(13)	Co1-N11_2	2.121(4)	Co2-N11_3	2.132(5)	Co1-N11	2.1637(16)
Co1-N51	2.0933(14)	Co1-N1_1	2.079(4)	Co2-N1_4	2.072(5)	Co1-N31	2.0919(14)
Co1-N62	2.1811(16)	Co1-N11_1	2.151(4)	Co2-N21_4a	2.184(16)	Co1-N41	2.1357(16)
Co1-N82	2.1788(15)	Co1-N21_1	2.139(5)	Co2-N11_4	2.162(5)	Co1-N51	2.1395(16)

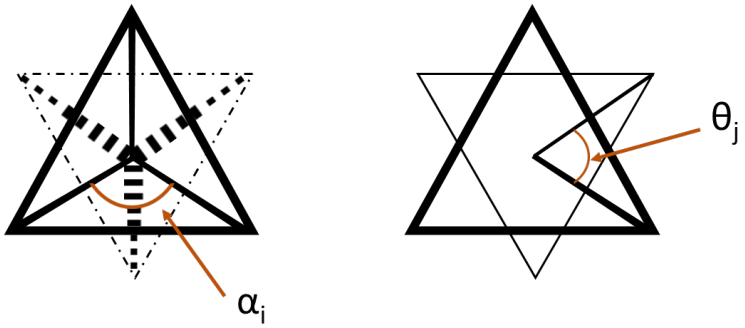

$$\Sigma = \sum_{i=1}^{12} |90 - \alpha_i|$$

$$\Theta = \sum_{j=1}^{24} |60 - \theta_j|$$

Scheme S2. Representation of angles used to calculate the distortion indices obtained by OctaDist Σ and Θ for an octahedral coordination complex following the next expressions.

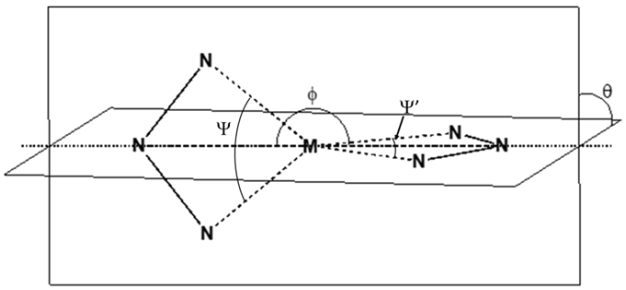

Scheme S3. Angles referred to Jahn–Teller distortion in Oh bis-tridentate complexes

*Table S3: Distortion indices and angles for Co^{II} complexes in **1**–**3** at 100 K. Σ and Θ are calculated and obtained from OctaDist software. Ψ is referred to the angle formed by $N_{triazole}$–Co–$N_{triazole}$, while ϕ is the angle between $N_{pyridine}$–Co–$N_{pyridine}$. θ is the angle between planes that contains the ligand atoms.*

Angle (°)	1	2_Co1	2_Co2	3
Σ	129.98(5)	133.41(6)	139.18(8)	145.32(5)
Θ	490.94(8)	443.92(7)	492.13(4)	487.69(3)
Ψ/Ψ'	151.41(9)/150.32(6)	150.70(7)/152.18(4)	151.50(9)/151.90(8)	150.15(6)/151.52(8)
ϕ	166.35(7)	173.22(1)	172.15(8)	169.14(1)
θ	91.35(4)	99.52(5)	80.19(8)	105.67(7)

*Table S4: Hydrogen bonding in **2** at 100 K. Note: Hydrogen bonds considering the disordered atoms are omitted. The subindex labelling corresponds to: **COOH** for those atoms belonging from the carboxylic acids; **W** for those belonging from water molecules; **Cl** for those coming from a perchlorate; and **Tz** for the N of the triazole ring.*

Bond	Donor-H (Å)	Acceptor-H (Å)	Donor-Acceptor (Å)	Angle (°)
$O_{COOH}29\_1$–H29_1 ⋯ O_W1_17a	0.84	1.70	2.427(16)	143
$O_{COOH}19\_2$–H19_2 ⋯ $O_{COOH}18\_1$	0.84	1.75	2.585(6)	172
$O_{COOH}29\_2$–H29_2 ⋯ O_W1_11	0.84	1.74	2.565(8)	168
$O_{COOH}29\_3$–H29_3 ⋯ O_W1_17a	0.84	1.64	2.443(14)	159
$O_{COOH}19\_4$–H19_4 ⋯ $O_{COOH}19\_1$	0.84	1.65	2.482(6)	169
O_W1_11–H1_11 ⋯ $O_{Cl}3\_5a$	0.96	2.06	2.982(10)	161
O_W1_11–H2_11 ⋯ $O_{COOH}18\_4$	0.96	1.81	2.742(8)	163
O_W1_12–H1_12 ⋯ O_W1_14	0.96	1.60	2.551(11)	173
O_W1_12–H2_12 ⋯ $O_{COOH}18\_3a$	0.96	1.63	2.541(9)	156
O_W1_12–H2_12 ⋯ $O_{COOH}19\_3a$	0.96	2.48	3.279(9)	141
O_W1_13–H1_13 ⋯ O_W1_12	0.96	1.88	2.734(9)	148
O_W1_13–H2_13 ⋯ $O_{COOH}19\_1$	0.96	1.85	2.789(8)	167
O_W1_14–H1_14 ⋯ $O_{COOH}18\_2$	0.96	2.36	3.267(10)	158
O_W1_14–H1_14 ⋯ $N_{Tz}22\_2$	0.96	2.53	2.892(11)	103
O_W1_14–H2_14 ⋯ $O_{COOH}28\_4a$	0.96	1.86	2.739(16)	151
O_W1_17a–H2_17a ⋯ $O_{Cl}4\_5a$	0.96	2.26	3.085(13)	144

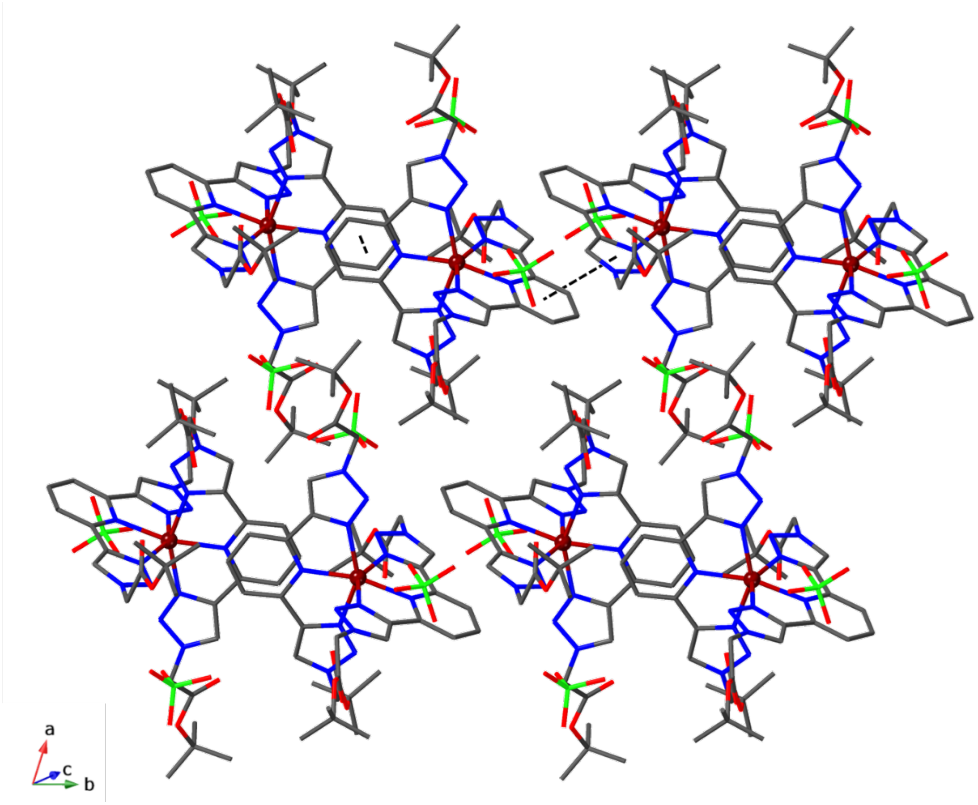

*Figure S20. Ball and stick representation for complex **1**, showing the perchlorate positions. Carbon, nitrogen, oxygen, chlorine and cobalt atoms are depicted in grey, blue, red, light green and brown, respectively. Dashed black lines represent stacking interactions.*

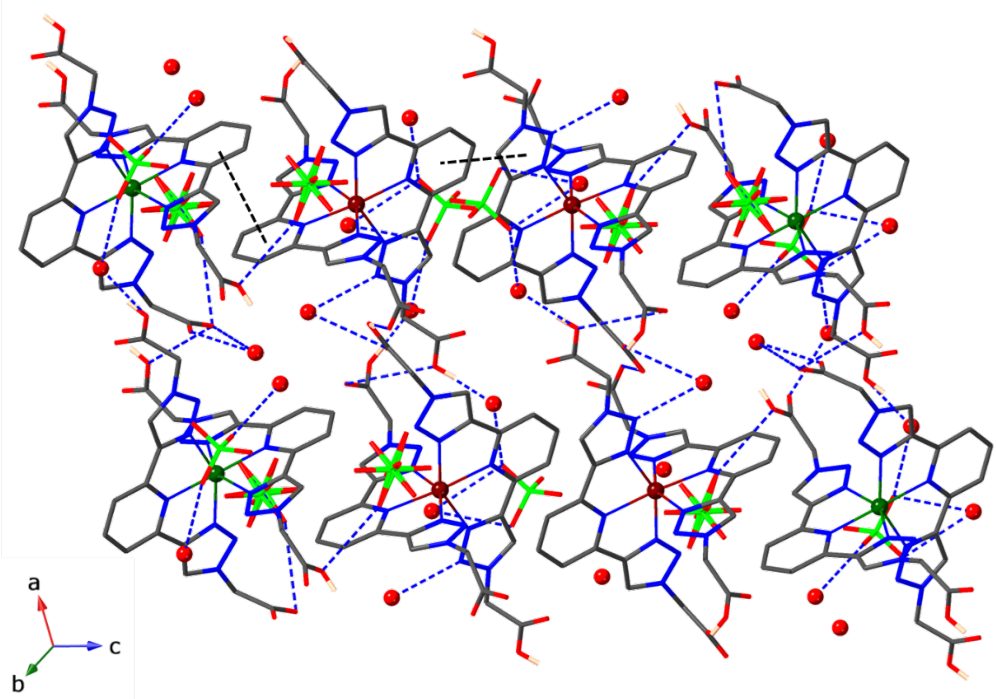

*Figure S21. Ball-and-stick representation of the packing of complex **2**, including the perchlorate positions. Carbon, nitrogen, oxygen and chlorine atoms are depicted in grey, blue, red and light green, respectively. Co_1 and Co_2 are depicted in brown and drank green, respectively. Red spheres represent water molecules. Dashed black and blue lines represent stacking interactions and hydrogen bonds, respectively.*

*Table S5: Hydrogen bonding in **3** at 100 K.* The subindex labelling corresponds to: **COOH** for those atoms belonging from the carboxylic acids and **W** for those belonging from water molecules.

Bond	Donor-H (Å)	Acceptor-H (Å)	Donor-Acceptor (Å)	Angle (°)
$O_{COOH}19$-H19···$O_{COOH}49$#1	0.95	1.51	2.435(2)	163
$O_{COOH}59$-H59···$O_{COOH}29$	0.88	1.69	2.569(2)	176
O_w1_1-H1_1···$O_{COOH}28$	0.96	1.90	2.851(3)	172
O_w1_1-H2_1···$O_{COOH}28$#4	0.956	2.01	2.944(3)	164
O_w1_2-H1_2···$O_{COOH}18$	0.96	1.94	2.877(3)	165
O_w1_2-H2_2···$O_{COOH}28$	0.958	2.051	2.984(3)	164
O_w1_3-H1_3···$O_{COOH}49$	0.96	1.79	2.739(2)	167.8
O_w1_3-H2_3···$O_{COOH}18$#3	0.957	2.19	2.983(2)	140

*Table S6: Intermolecular Co···Co distances for complexes **1-3** at 100 K.*

Compound	Intra-layer M···M distances (Å)	Inter-layer M···M distances (Å)
1	7.63(6)/8.25(4)/11.28(8)	13.97(8)
2	7.79(1)/7.89(7)/8.17(6)/10.87(8)	11.39(4)/11.04(1)
3	7.31(1)/7.58(7)/7.72(2)	12.86(7)

*Table S7. Main π-π interactions for complex **1** considering centroid-centroid distances.*

Centroids	Distance (Å)	Alpha (°)	Slippage (Å)
Cg_{py}–Cg_{pz}	3.9556(10)	1.53(9)	1.943
Cg_{py}–Cg_{py}	3.628(9)	0.00(8)	1.273

*Table S8. Main π-π interactions for complex **2** considering centroid-centroid distances.*

Centroids	Distance (Å)	Alpha (°)	Slippage (Å)
Cg_{pz1}–Cg_{py1}	4.096(3)	4.6(3)	2.332
Cg_{py1}–Cg_{py2}	3.947(4)	1.4(3)	1.878
Cg_{py1}–Cg_{py1}	3.776(3)	0.0(3)	1.790
Cg_{pz2}–Cg_{py2}	4.071(4)	5.2(3)	2.105
Cg_{py2}–Cg_{py2}	4.046(4)	0.0(3)	2.138

*Table S9. Main π-π interactions for complex **3** considering centroid-centroid distances.*

Centroids	Distance (Å)	Alpha(°)	Slippage (Å)
Cg_{pz}–Cg_{py}	3.6464(11)	2.38(10)	1.009
Cg_{pz}–Cg_{py}	3.5971(11)	12.57(10)	0.894
Cg_{py}–Cg_{py}	3.6028(11)	0.03(9)	1.268

Magnetic studies

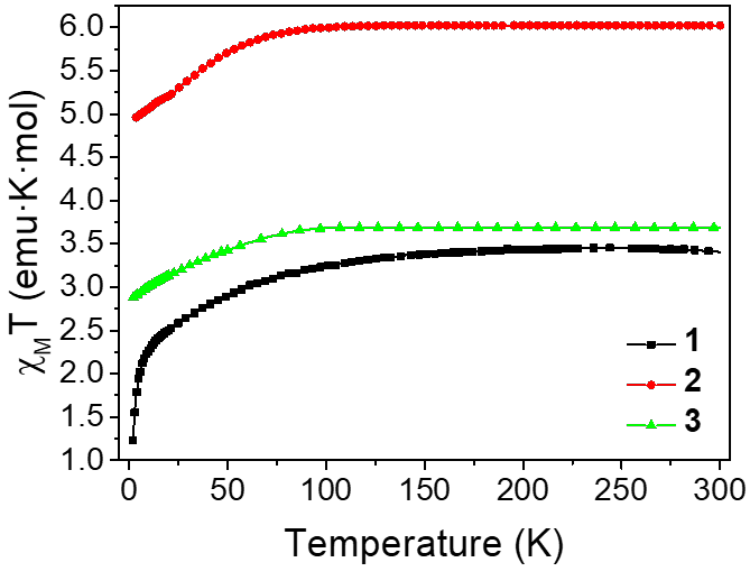

*Figure S22: Temperature dependence of $\chi_M T$ for **1**–**3** in the temperature range between 2 and 300 K on cooling mode with a scan rate of 2 K·min^{-1} under an applied magnetic field of 1T for **1** and 0.1 T for **2** and **3**.*

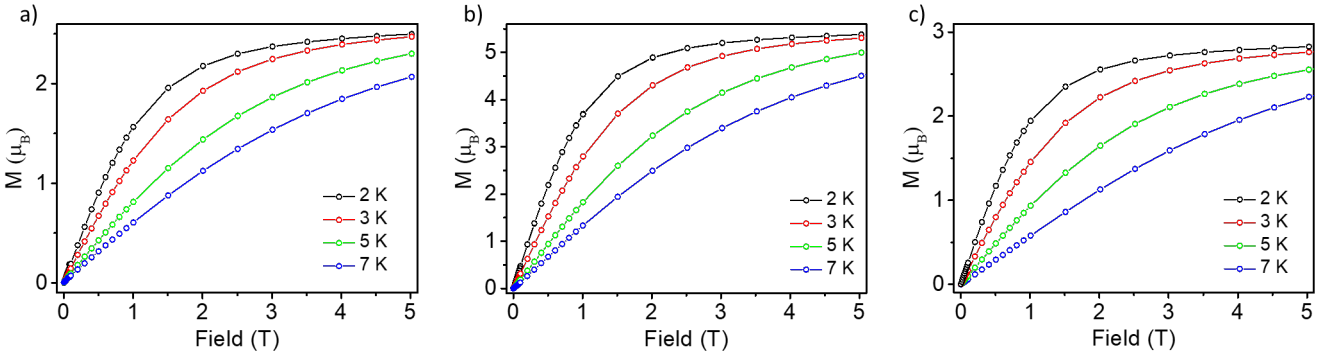

*Figure S23: Field dependence of the magnetization of **1** (a), **2** (b) and **3** (c) at different temperatures between 2–7K.*

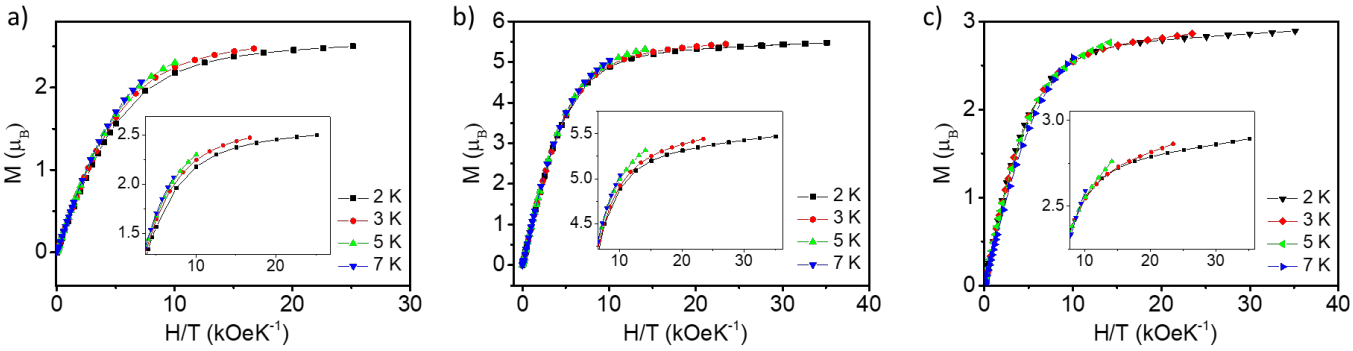

*Figure S24: Isothermal reduced magnetization at different temperatures between 2–7K for **1** (a), **2** (b) and **3** (c). Inset: M vs H/T plot in the high applied magnetic field region to illustrate the non-superposition of the curves.*

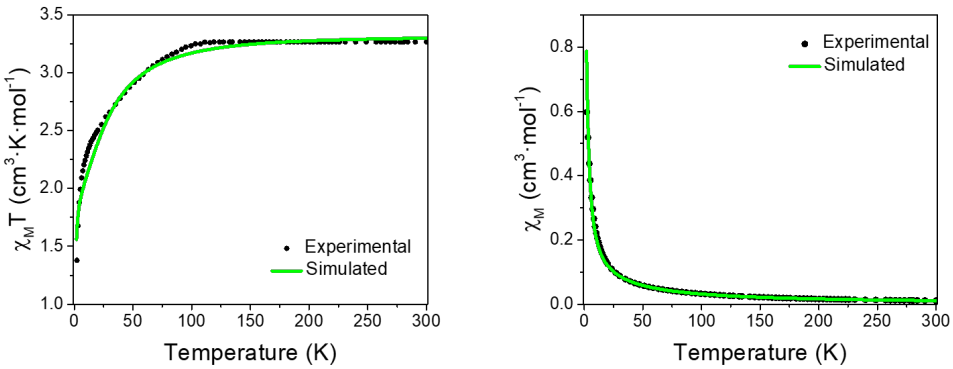

*Figure S25. Fitted susceptibility curves extracted from PHI software for compound **1**. Dots represents the experimental data, while lines the fitting.*

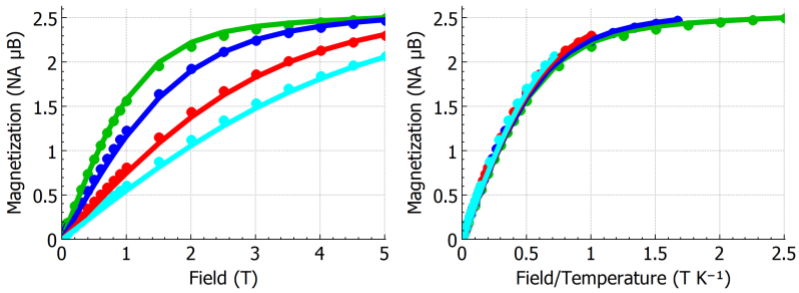

Figure S26. Fitted magnetization and reduced magnetization extracted from PHI software for compound 1. Dots represents the experimental data, while lines the fitting.

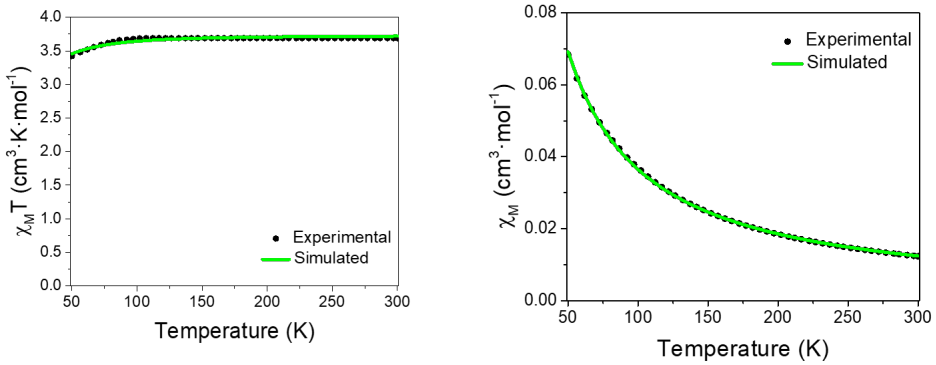

*Figure S27. Fitted susceptibility curves extracted from PHI software for compound **3**. Dots represents the experimental data, while lines the fitting.*

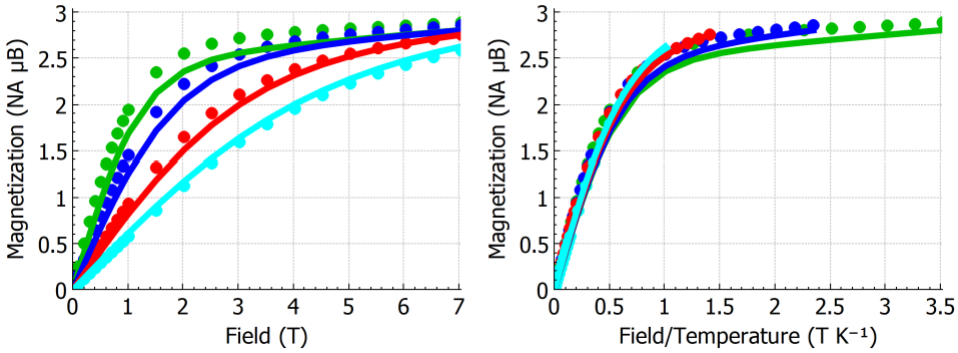

Figure S28. Fitted magnetization and reduced magnetization extracted from PHI software for compound 1. Dots represents the experimental data, while lines the fitting.

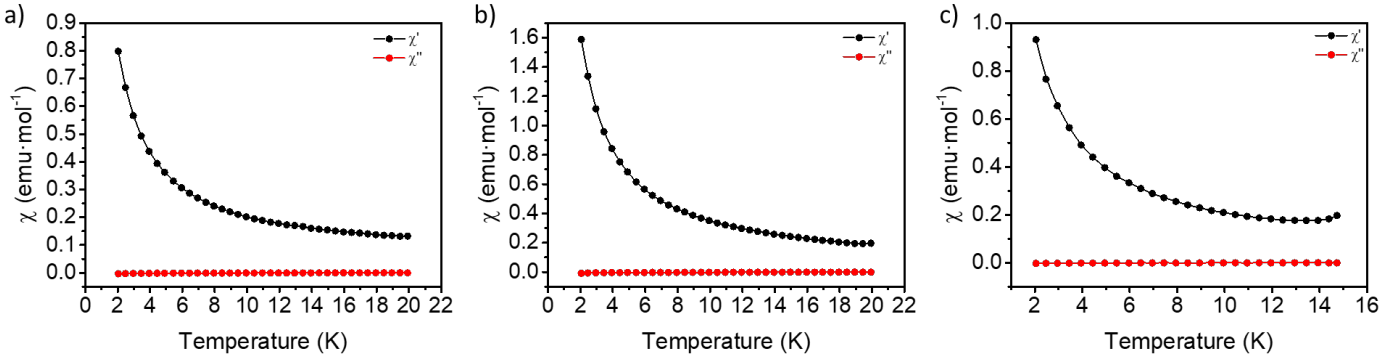

*Figure S29: Temperature dependence in-phase (black) and out-of-phase (red) ac susceptibility for **1** (a), **2** (b) and **3** (c) at 10 kHz under a dc applied magnetic field of 0 T.*

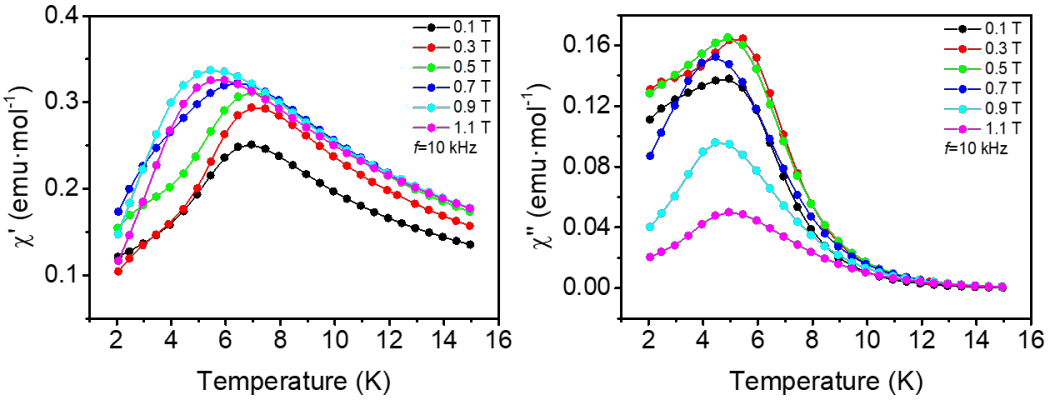

*Figure S30: Temperature dependence in-phase (χ') and out-of-phase (χ'') ac susceptibility for **1** under different applied magnetic fields (0.1–1.1 T) at a frequency of 10 kHz.*

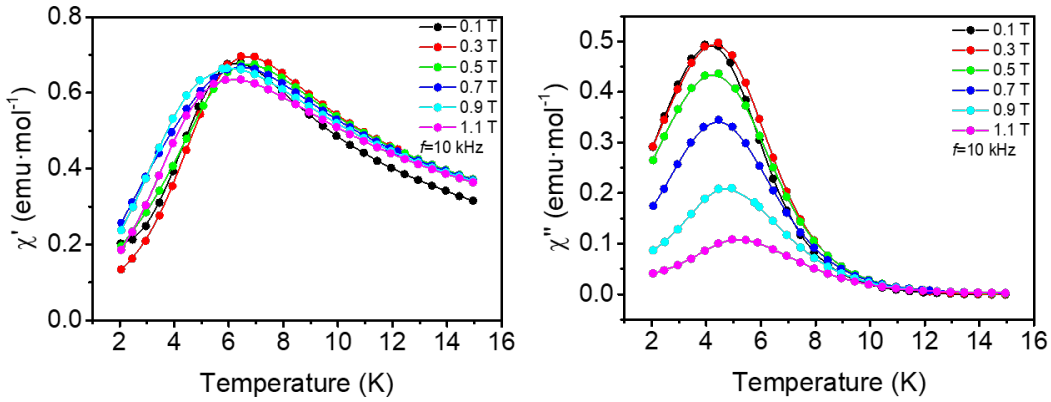

*Figure S31: Temperature dependence in-phase (χ′) and out-of-phase (χ″) ac susceptibility for **2** under different applied magnetic fields (0.1–1.1 T) at a frequency of 10 kHz.*

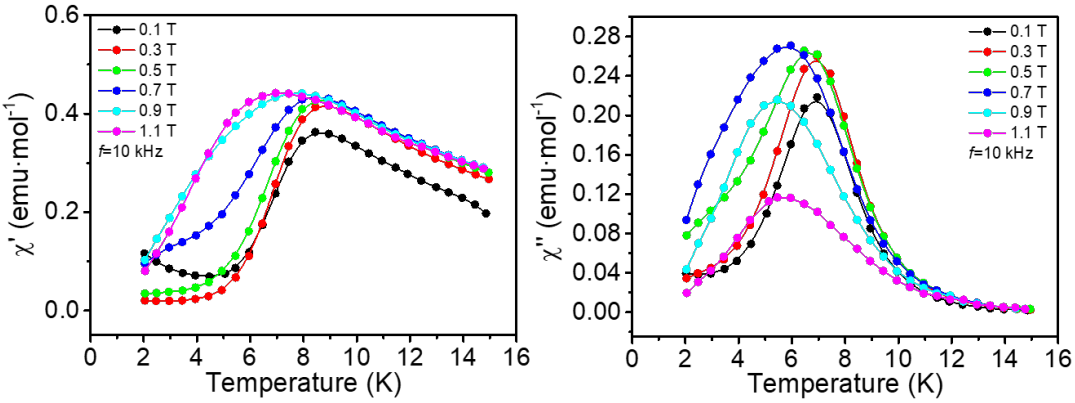

*Figure S32: Temperature dependence in-phase (χ′) and out-of-phase (χ″) ac susceptibility for **3** under different applied fields (0.1–1.1 T) at a frequency of 10 kHz.*

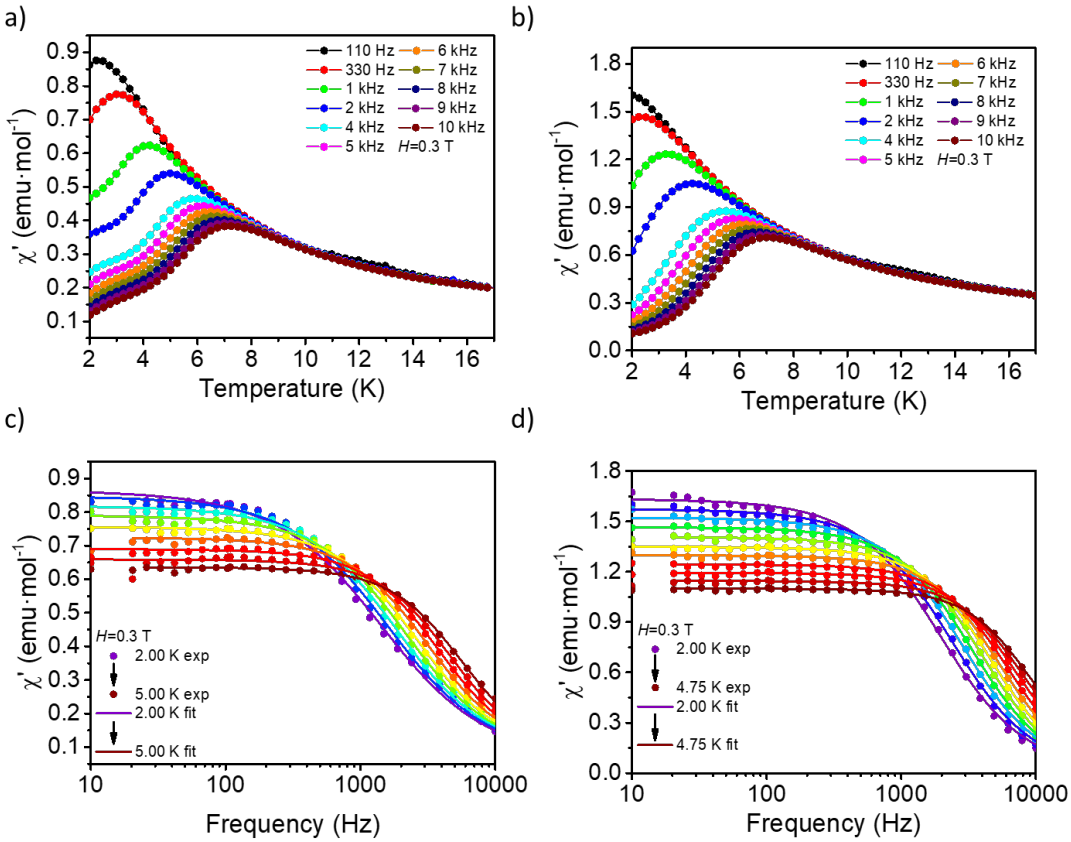

*Figure S33: Temperature dependence in-phase (χ') ac susceptibility under an applied magnetic field of 0.3 T in the frequency range between 110 Hz–10 kHz for **1** (a) and **2** (b). Frequency dependence in-phase (χ') ac susceptibility under an applied magnetic field of 0.3 T in the temperature range of 2–5 K for **1** (c) and **2** (d). Fitted curves as solid lines.*

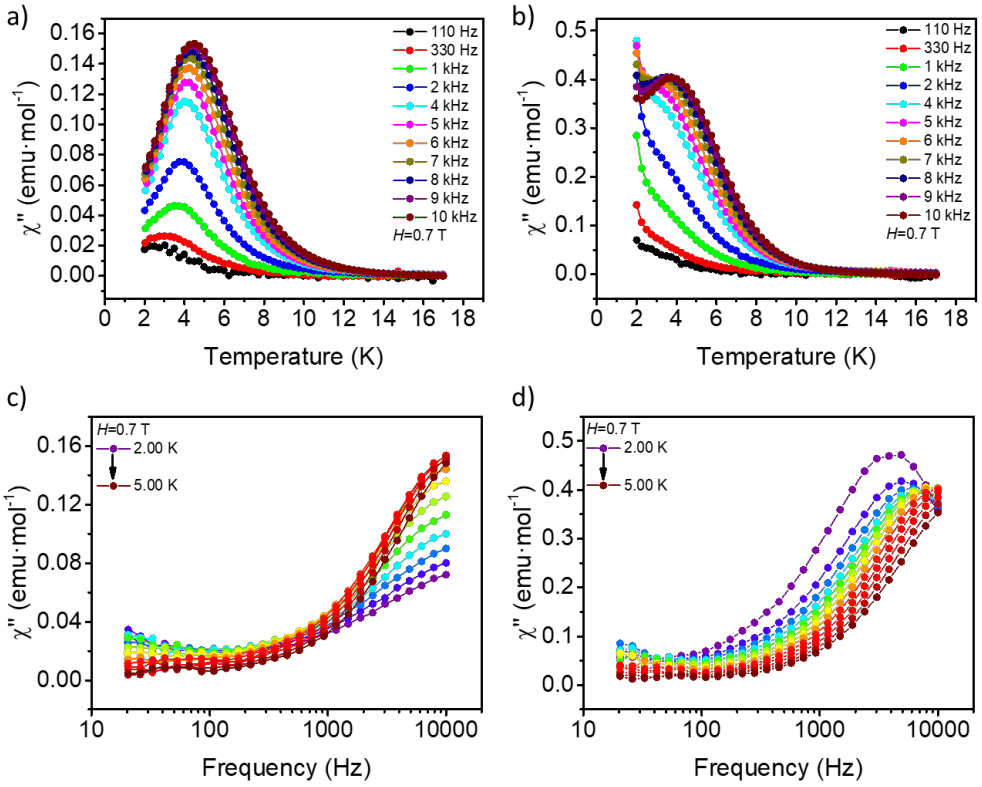

*Figure S34. Temperature dependence out-of-phase (χ'') susceptibility under an applied magnetic field of 0.7 T in the frequency range between 110 Hz–10 kHz for **1** (a) and **2** (b). Frequency dependence out-of-phase (χ'') ac susceptibility under an applied magnetic field of 0.7 T in the temperature range of 2–5 K for **1** (c) and **2** (d).*

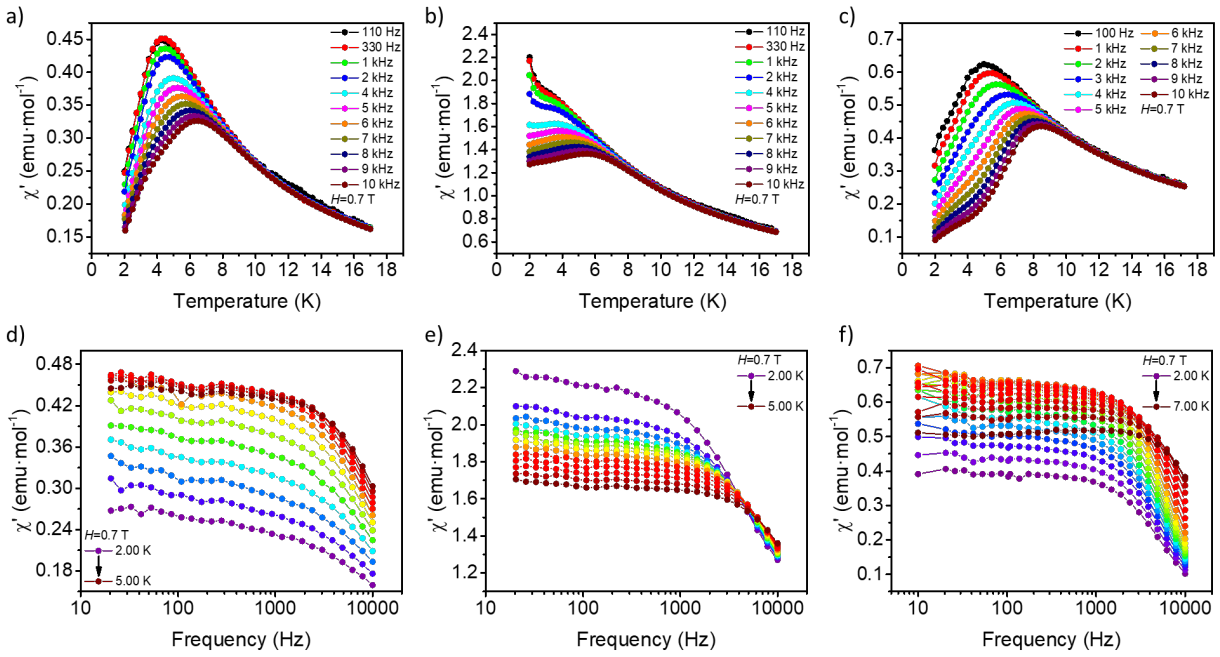

*Figure S35. Temperature dependence in-phase (χ') ac susceptibility under an applied magnetic field of 0.7 T in the frequency range between 110 Hz–10 kHz for **1** (a), **2** (b) and **3** (c). Frequency dependence in-phase (χ') ac susceptibility under an applied field of 0.7 T in the temperature range of 2–5 K for **1** (d), **2** (e) and **3** (f).*

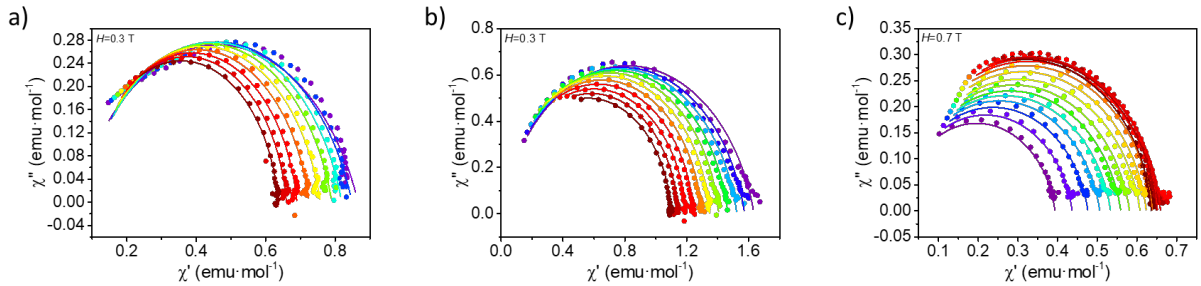

*Figure S36. Cole-Cole plots under an applied dc magnetic field in the temperature range 2–5 K for **1** (a) 2–4.75 K for **2** (b), and in the temperature range between 2–5.75 K for **3** (c). Fitted curves as solid lines.*

*Table S10. Relaxation fitting parameters from the least-square fitting of the Cole-Cole plots for **1**–**3** according to the generalized Debye model at 0.3 T for **1** and **2**, and at 0.7 T for **3**.*

1				
T (K)	**χ_S (cm^3 mol^{-1})**	**χ_T (cm^3 mol^{-1})**	**τ (s)**	**α**
3.001187	0.0563001306	0.866155278	1.11168753E-04	0.246470147
3.250568	0.0688645729	0.848578504	9.87825385E-05	0.213864026
3.500596	0.0777292505	0.819049996	8.48956498E-05	0.183599559
3.749849	0.0784387670	0.790417202	7.18958289E-05	0.165641442
3.999169	0.0810555493	0.757079879	6.00781576E-05	0.143266333
4.249762	0.0818941326	0.724634324	4.99163294E-05	0.124730228
4.498618	0.0860823034	0.689950592	4.15588017E-05	0.0994364276
4.747745	0.0851043535	0.659373654	3.44345728E-05	0.0835061529
4.999624	0.0778907716	0.636219191	2.83828575E-05	0.0845257324
2				
T (K)	**χ_S (cm^3 mol^{-1})**	**χ_T (cm^3 mol^{-1})**	**τ (s)**	**α**
2.01174	6.325E-18	1.62887	8.14847E-5	0.15441
2.25537	2.51924E-18	1.56834	6.70025E-5	0.13788
2.50524	1.56988E-19	1.51799	5.60378E-5	0.12319
2.75062	3.71038E-22	1.46064	4.7235E-5	0.10634
3.00052	7.92307E-15	1.4023	4.0021E-5	0.09187
3.24964	3.80909E-20	1.34426	3.42463E-5	0.07917
3.49973	3.1181E-17	1.29351	2.96162E-5	0.07351
3.74935	0.00718	1.2392	2.57767E-5	0.0625
3.9987	0.0097	1.18991	2.2383E-5	0.05922
4.24904	0.02088	1.14127	1.97768E-5	0.04972
4.49824	0.0247	1.09563	1.73191E-5	0.0463
3				
T (K)	**χ_S (cm^3 mol^{-1})**	**χ_T (cm^3 mol^{-1})**	**τ (s)**	**α**
2.00244	7.3666E-17	0.396	3.08342E-5	0.09894
2.25252	1.40087E-18	0.43972	3.09004E-5	0.10808
2.50171	1.21358E-16	0.47949	3.10257E-5	0.11442
2.75135	7.08214E-17	0.50962	3.07324E-5	0.11452
3.0005	2.13023E-15	0.53714	3.04547E-5	0.11826
3.25006	1.98659E-15	0.56316	3.01807E-5	0.12267
3.49966	3.27209E-17	0.58511	2.97254E-5	0.11643
3.74893	2.12584E-20	0.61205	2.95287E-5	0.11705
3.99857	8.29663E-17	0.62763	2.86262E-5	0.09798
4.24807	1.5201E-16	0.64365	2.7738E-5	0.08674
4.4978	4.27846E-18	0.65628	2.66389E-5	0.07994
4.74715	1.37926E-18	0.66366	2.52679E-5	0.07602
4.9969	1.06053E-13	0.66383	2.35209E-5	0.06823
5.24595	2.88923E-20	0.66345	2.17601E-5	0.06978
5.49558	2.30283E-13	0.65369	1.97567E-5	0.06283
5.74544	1.94679E-13	0.64016	1.77688E-5	0.05655

*Table S11. Best-fit parameters of Orbach relaxation processes fitting by Arrhenius law for **1**–**3***

	τ_0 (s)	U_{eff}/k_B (cm^{-1})
1	$1.14E^{-06}$	16.11
2	$2.46E^{-06}$	8.82
3	$3.39E^{-06}$	9.64

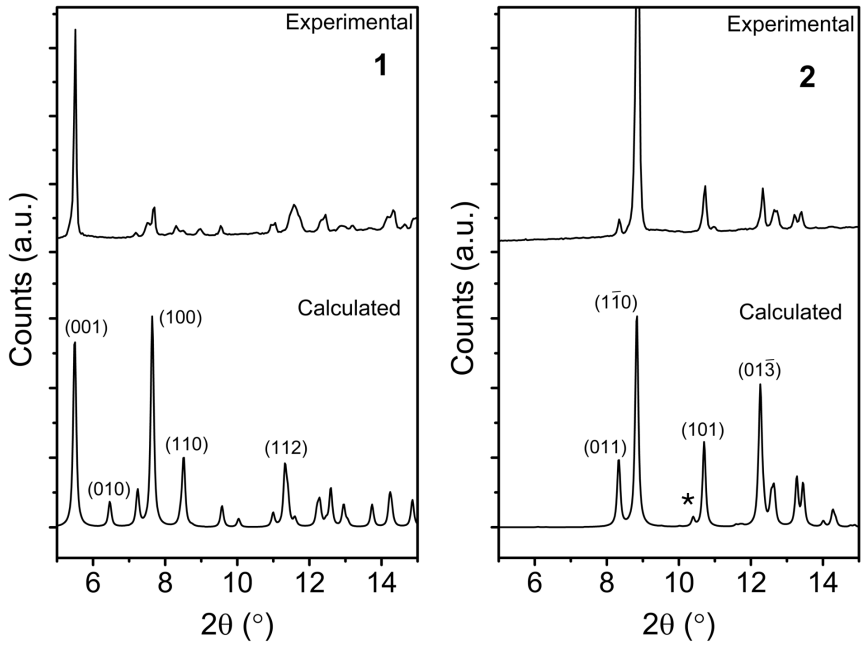

*Figure S37. Powder X-ray diffraction measurements for compounds **1** and **2** were performed on the ground samples after magnetic measurements and were compared with the simulated data from single-crystal X-ray diffraction measurements obtained at 100 K (CCDC-2281065 for **1** and CCDC-2281066 for **2**). It is worth noting that a SQUEEZE procedure was applied in CCDC-2281065. Therefore, the simulated data for **1** does not provide information about the solvated molecules. Powder diffractograms calculated from single-crystal data of **1** as a function of the solvent content in the cavity by progressively adding electron density peaks inside the cavity in the Fourier difference maps showed that the intensity of the (100), (010), and (110) peaks decreases, while intensity of the (001) peak is barely affected. As the cavity fills by adding electron density peaks, the calculated diffractogram becomes more similar to the one obtained experimentally from the ground samples whose magnetic properties were measured ("Experimental"). For compound **2**, the small additional peak marked with an asterisk may be attributed to the presence of a minor impurity.*

References:

1- F. Lloret, M. Julve, J. Cano, R. Ruiz-García and E. Pardo, Inorg. Chim. Acta, 2008, 361, 3432–3445.